Received: 16 February 2023 | Revised: 12 August 2023 | Accepted: 25 August 2023

DOI: 10.1002/pld3.531

RESEARCH ARTICLE

Blue-green fluorescence during hypersensitive cell death arises from phenylpropanoid deydrodimers

Basem Kanawati[1] | Marko Bertic[2] | Franco Moritz[1] | Felix Habermann[3] | Ina Zimmer[2] | David Mackey[4] | Philippe Schmitt-Kopplin[1] | Jörg-Peter Schnitzler[2] | Jörg Durner[5] | Frank Gaupels[5]

[1]Analytical BioGeoChemistry, Helmholtz Zentrum München, Neuherberg, Germany

[2]Research Unit Environmental Simulation, Institute of Biochemical Plant Pathology, Helmholtz Zentrum München, Neuherberg, Germany

[3]Institute of Anatomy, Histology and Embryology, Department of Veterinary Sciences, Ludwig-Maximilians-University Munich, Munich, Germany

[4]Department of Horticulture and Crop Science and Department of Molecular Genetics, Ohio State University, Columbus, Ohio, USA

[5]Institute of Biochemical Plant Pathology, Helmholtz Zentrum München, Neuherberg, Germany

Correspondence
Frank Gaupels, Institute of Biochemical Plant Pathology, Helmholtz Zentrum München, Neuherberg D-85764, Germany.
Email: frank.gaupels@gmx.de

Funding information
None.

Abstract

Infection of Arabidopsis with avirulent *Pseudomonas syringae* and exposure to nitrogen dioxide (NO_2) both trigger hypersensitive cell death (HCD) that is characterized by the emission of bright blue-green (BG) autofluorescence under UV illumination. The aim of our current work was to identify the BG fluorescent molecules and scrutinize their biosynthesis, localization, and functions during the HCD. Compared with wild-type (WT) plants, the phenylpropanoid-deficient mutant *fah1* developed normal HCD except for the absence of BG fluorescence. Ultrahigh resolution metabolomics combined with mass difference network analysis revealed that WT but not *fah1* plants rapidly accumulate dehydrodimers of sinapic acid, sinapoylmalate, 5-hydroxyferulic acid, and 5-hydroxyferuloylmalate during the HCD. FAH1-dependent BG fluorescence appeared exclusively within dying cells of the upper epidermis as detected by microscopy. Saponification released dehydrodimers from cell wall polymers of WT but not *fah1* plants. Collectively, our data suggest that HCD induction leads to the formation of free BG fluorescent dehydrodimers from monomeric sinapates and 5-hydroxyferulates. The formed dehydrodimers move from upper epidermis cells into the apoplast where they esterify cell wall polymers. Possible functions of phenylpropanoid dehydrodimers are discussed.

KEYWORDS
5-hydroxyferulic acid, autofluorescence, cell wall, dehydrodimers, *fah1*, hypersensitive cell death, sinapic acid

1 | INTRODUCTION

Infection of *Arabidopsis thaliana* with avirulent *Pseudomonas syringae* pv. *tomato* expressing the avirulence gene *AvrRpm1* (*P.s.t. AvrRpm1*) triggers the hypersensitive defense response (HR) culminating in programmed cell death (PCD) (Coll et al., 2011; Katagiri et al., 2002). HR-PCD can be distinguished from other forms of PCD by the appearance of UV-induced blue-green (BG) fluorescence in dying leaf tissues (Bennett et al., 1996; Nicholson & Hammerschmidt, 1992). HR-PCD depends on simultaneous signaling by reactive oxygen- and nitrogen species (Delledonne et al., 2001; Gaupels et al., 2011). Exposure of Arabidopsis to nitrogen dioxide (NO_2) results in basal

Basem Kanawati and Marko Bertic contributed equally to this article.

pathogen immunity or rapid cell death in a dose-dependent manner (Kasten et al., 2016; Mayer et al., 2018). NO_2-induced cell death is accompanied by the strong emission of BG fluorescence under UV light similar to HR-PCD (Frank et al., 2019). Hereafter, NO_2- and *P.s.t. AvrRpm1*-induced cell death will be collectively called hypersensitive cell death (HCD).

The enigmatic BG fluorescence under UV illumination was recognized long ago (Nicholson & Hammerschmidt, 1992). However, even after more than 40 years of intense research, the source of the fluorescence remains ambiguous. Based on microscopy and spectral analyses, phenolic compounds such as phenylpropanoids might be a major source of autofluorescence during the HCD without individual molecules identified to date (Nicholson & Hammerschmidt, 1992). In Arabidopsis, sinapic acid (Si) and sinapoylmalate (SM) are the dominant phenylpropanoids mainly localized in the leaf upper epidermis where they act as a sunscreen by scavenging harmful UV irradiation under emission of blue fluorescence (Chapple et al., 1992; Milkowski & Strack, 2010). Preliminary experiments revealed that the HCD-related BG fluorescence and the blue fluorescence of sinapates co-localized in the upper epidermis.

These findings prompted us to investigate HCD in mutants deficient in phenylpropanoids. *pal1/2* has low levels of phenylpropanoids due to mutation of *PAL1* and *PAL2* (Rohde et al., 2004). Both genes code for phenylalanine ammonia lyases (PAL) that catalyze the initial reaction of the phenylpropanoid pathway, namely, the synthesis of cinnamic acid from phenylalanine (Fraser & Chapple, 2011). The PAL activity is reduced by 75% and the level of total soluble phenolics by 66% in the *pal1/2* double mutant (Rohde et al., 2004). *FAH1* codes for the enzyme ferulate-5-hydroxylase (F5H) that converts ferulic acid into 5-hydroxyferulic acid (Hf), the latter being subsequently O-methylated to Si (Fraser & Chapple, 2011). F5H also converts coniferaldehyde and coniferylalcohol into their 5-hydroxy derivatives. However, the most prominent phenotype of the *fah1* mutant is its deficiency in Hf and Si.

The results of our study with the *pal1/2* and *fah1* mutant lines suggest that derivatives of Si and its precursor 5-hydroxyferulic acid (Hf) form BG fluorescent dehydrodimers. Additionally, we scrutinized

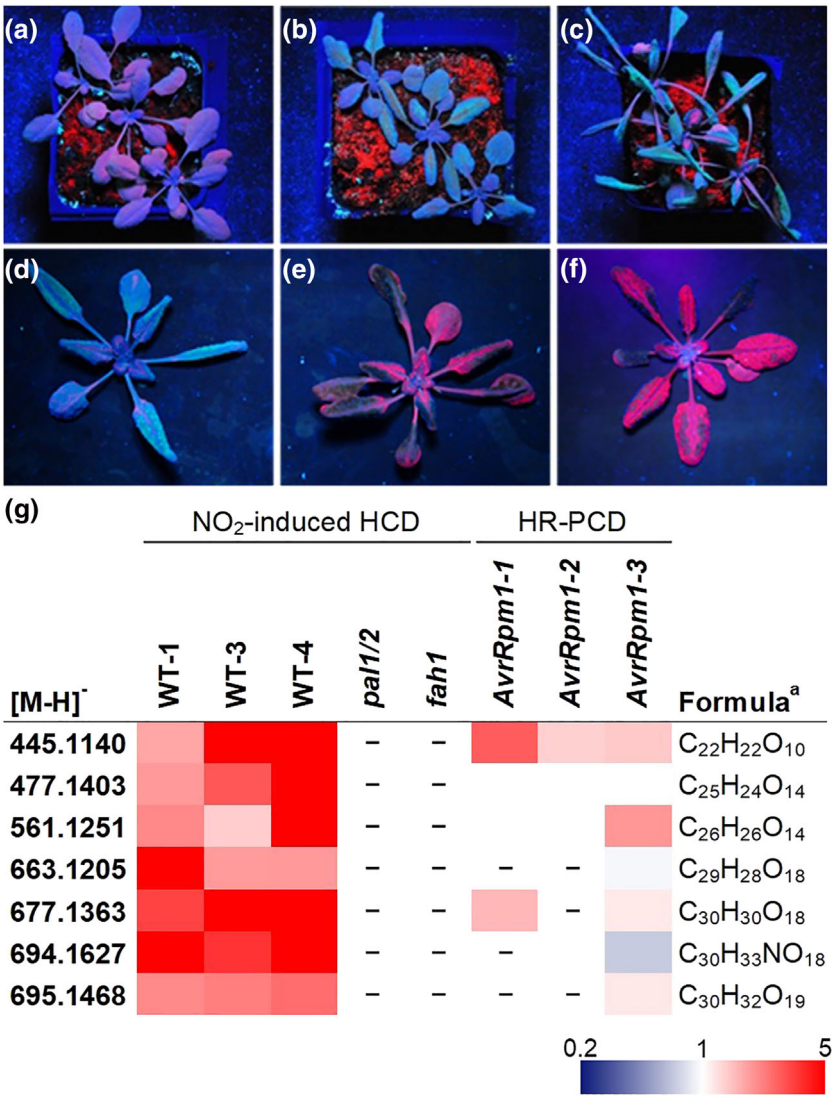

FIGURE 1 The mutants *fah1* and *pal1/2* do not show blue-green (BG) fluorescence during the hypersensitive cell death (HCD). Plants were observed under UV light for fluorescence emission from chlorophyll (red) and phenolic secondary metabolites (BG). (a) Untreated Arabidopsis wild-type (WT) plants. (b) *Dex::AvrRpm1* transgenic plants 3 h after induction of hypersensitive response-related programmed cell death (HR-PCD) by spraying dexamethasone solution. (c and d) Arabidopsis WT plants immediately after fumigation for 1 h with 30-ppm NO_2. (e) *pal1/2* and (f) *fah1* mutant plants after NO_2 treatment. *pal1/2* has reduced levels of phenylpropanoids. *fah1* is deficient in 5-hydroxyferulic acid (Hf) and sinapic acid (Si). (g) Leaf extracts were analyzed by non-targeted Fourier transform ion cyclotron resonance mass spectrometry (FT-ICR-MS). The figure depicts unknown metabolites accumulating in all three NO_2 fumigation experiments but not detected in *pal1/2* or *fah1*. Red and blue shades indicate significantly increased or decreased spectral counts (fold change), respectively. White color indicates not significantly regulated and white plus dash not detected. Please refer to File S1 for original data including statistics. [a]Sum formula of uncharged molecule.

the mechanism of formation and possible functions of the phenylpropanoid dehydrodimers.

2 | RESULTS

2.1 | BG autofluorescence is dependent on sinapates and 5-hydroxyferulates

Leaves of untreated Arabidopsis plants emit red chlorophyll fluorescence and blue fluorescence under UV illumination (Figure 1a). The blue fluorescence originates from sinapates localized in the upper leaf epidermis (Milkowski & Strack, 2010). For the investigation of HR-PCD, we used transgenic Arabidopsis expressing the *P.s.t.* avirulence gene *AvrRpm1* under control of a dexamethasone (Dex)-inducible promoter that allows the reproducible initiation of HR without a pathogen (Mackey et al., 2002). Spraying *Dex::AvrRpm1* plants with Dex elicited rapid cell death, leaf collapse, and the emission of bright BG fluorescence at 3 h after treatment (Figure 1b). Fumigation for 1 h with 30-ppm NO_2 led to rapid cell death, leaf collapse, and strong BG fluorescence immediately after the treatment (Figure 1c,d).

By contrast, the Si- and Hf-deficient knock-out mutants *pal1/2* (Figure 1e) and *fah1* (Figure 1f) undergo NO_2-induced PCD but do not show blue or BG fluorescence when inspected under UV. Hence, BG fluorescence in dying leaf tissues is dependent on Hf and Si. However, the induction of HCD is independent of BG fluorescence, Hf, and Si.

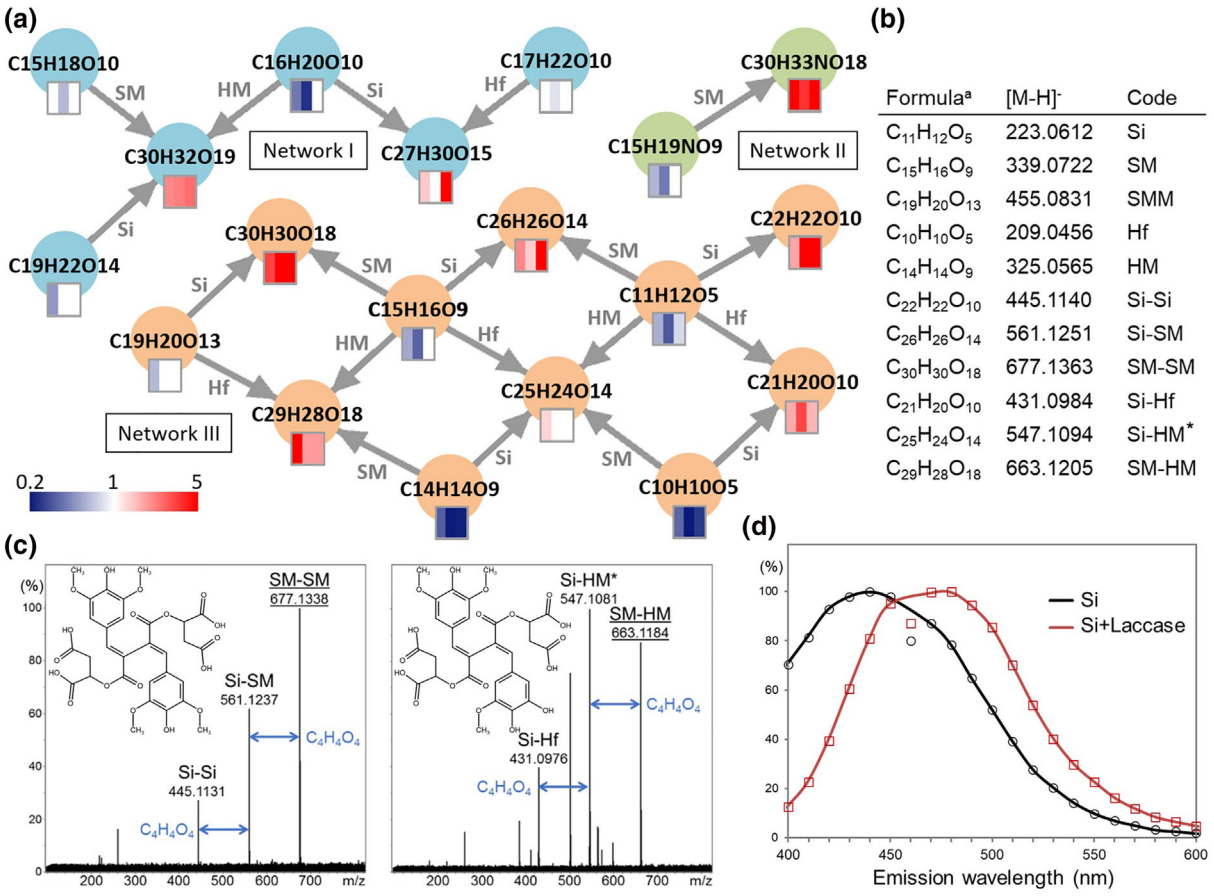

FIGURE 2 Dehydrodimers of sinapates and 5-hydroxyferulates accumulate during NO_2-induced cell death. (a) Mass difference network (MDN) analysis. Accurate negative ion masses as determined by Fourier transform ion cyclotron resonance mass spectrometry (FT-ICR-MS) were analyzed for mass differences due to binding of dehydrogenated sinapic acid (Si), sinapoylmalate (SM), 5-hydroxyferulic acid (Hf), and 5-hydroxyferuloylmalate (HM) (for complete datasets, see File S1). The node colors indicate different sub-networks. Square icons depict the NO_2-induced regulation in three independent experiments. The color code represents fold change in spectral count (NO_2/air ratio). White color means not detected or not regulated (for data and statistics, see File S1). (b) Chemical formulae of the uncharged molecules, measured accurate masses of the $[M-H]^-$ ions, and code describing the monomers and dimers found in network III shown in (a). (c) Tandem mass spectrometry fragmentation patterns at a collision energy of 8 eV of the SM-SM and SM-HM dehydrodimers. Parent ions are underlined. Representative structures of 8–8-coupled SM-SM and SM-HM dimers are shown. The loss of malyl ($C_4H_4O_4$) moieties during the fragmentation is indicated by blue arrows. The full peak lists can be found in Figure S1. (d) Fluorescence spectra of Si alone and Si after laccase addition causing the formation of Si-Si dehydrodimers. The excitation wavelength was 320 nm. *Si-HM or SM-Hf. [a]Sum formula of uncharged molecule.

2.2 | Dehydrodimerization of phenylpropanoids is a source of BG fluorescence

The *pal1/2* and *fah1* mutant lines were further employed to identify BG fluorescent metabolites by direct-infusion Fourier transform ion cyclotron resonance mass spectrometry (FT-ICR-MS), a technique that facilitates the determination of molecular masses with sub-ppm accuracy (<.001 Da). Accurate masses can then be used to calculate the chemical formulae and generate putative annotations. This non-targeted metabolomics approach detected seven metabolites that showed increased levels after NO_2 exposures of WT plants but were absent in *fah1* and *pal1/2* (Figure 1g). One metabolite with the negative ion mass ($[M-H]^-$) 445.1140 Da accumulated also upon induction of HR-PCD. In previous studies, compounds with similar measured masses were identified as sinapate dehydrodimers (Bunzel et al., 2003; Frolov et al., 2013; Yin et al., 2019) suggesting that HCD is accompanied by dimer formation between phenylpropanoids and, more specifically, between 5-hydroxyferulates and sinapates. SM, Si, 5-hydroxyferuloylmalate (HM), and Hf are the most abundant FAH1-dependent metabolites in Arabidopsis leaf extracts (File S1).

Dehydrodimerization involves one electron oxidation of the monomeric precursors to give dehydrogenated radicals (Bunzel, 2010; Ralph et al., 2004). Therefore, the FT-ICR-MS data were further scrutinized by mass difference network (MDN) analysis assuming that a dehydroradical of either SM, Si, HM, or Hf reacted with another unknown radical (Figure 2a). This approach uncovered possible molecular interactions (File S1). Three generated networks contained metabolites that were consistently regulated in all NO_2 fumigation experiments (Figure 2a). According to network I, the compound with the sum formula $C_{30}H_{32}O_{19}$ could arise from dehydrodimerization of Si, SM, or HM radicals with three different binding partners. $C_{16}H_{20}O_{10}$ might represent 5-hydroxyferulate glucose (HG) because it does not occur in *fah1*. In this case, $C_{30}H_{32}O_{19}$ that is also absent in *fah1* could refer to the HM-HG dehydrodimer. In network II, both the precursor $C_{15}H_{19}NO_9$ and the putative dehydrodimer $C_{30}H_{33}NO_{18}$ did not result in meaningful database hits.

The monomeric precursors depicted in network III likely correspond to Si, SM, sinapoyldimalate (SMM), Hf, and HM (Figure 2a,b) because they were highly abundant in WT but absent or strongly depleted in *fah1* and *pal1/2* (File S1). The spectral counts of the monomers mostly decreased upon NO_2 fumigation. MS/MS fragmentation analyses confirmed the identities of SM and SMM (Figure S1A,B). Network III suggests the formation of Si-Si, Si-SM, SM-SM, Si-Hf, Si-HM or SM-Hf (isomers not distinguishable), and SM-HM upon HCD induction (Figure 2a,b). Five dehydrodimers accumulated up to 10-fold in all experiments, whereas the levels of Si-HM/SM-Hf were generally low (File S1). MS/MS fragmentation analysis confirmed the identity of the SM-SM and SM-HM dimers (Figure 2c, Figure S1C,D), the most prominent fragmentation pattern being losses of the malyl moieties. Dehydrodimers of ferulates were not regulated during the HCD (File S1).

Next, we assessed whether the rise of dehydrodimers could explain the observed BG fluorescence emission during HCD. Peroxidases and laccase are known to catalyze polymerizations of phenolic compounds (Ralph et al., 2004; Tufegdžić et al., 2005). Si fluoresced blue under UV-A (320 nm) illumination. However, upon addition of laccase, the fluorescence turned BG (Figure 2d). The pronounced shift of the fluorescence maximum from 440 to 470 nm probably reflects dimerization of Si and is likely due to the increased size of the π conjugated system in the formed dehydrodimers. A similar shift in fluorescence was previously observed upon dehydrodimerization of ferulate (Tufegdžić et al., 2005).

2.3 | Fluorescent phenylpropanoid dehydrodimers arise within epidermal cells next to dying mesophyll cells

Untreated plants displayed UV-excited blue fluorescence in the adaxial epidermis but not the abaxial epidermis that lacks Si and Hf derivatives (Figure S2A,B). Fumigation with 30-ppm NO_2 for 20 min led to a transient increase in red fluorescence due to disturbed photosynthesis (Mayer et al., 2018) and rapid development of BG fluorescent lesions (Figure 3a). At 24 h after treatment, cells at the edge of the lesion appeared bright blue, whereas cells in the center of the lesion were BG fluorescent or non-fluorescent (Figure 3a,b). Mesophyll cells turned chlorotic during the HCD (Figure 3c). The bright blue fluorescence was particularly high in the cell peripheries (Figure 3d). Close examinations revealed that the BG fluorescence in the lesion centers vanished during HCD progression (Figure 3e). Infection with *P.s.t. AvrRpm1* also triggered the emission of bright blue and BG fluorescence during the HR (Figure 3f). Both the bright blue and BG fluorescence were not observed in *fah1* (Figure 3g–i) suggesting that they are related to the dehydrodimerization of Si- and Hf derivatives (Figures 1 and 2). It is yet unclear whether the BG and bright blue fluorescence emissions are related to different FAH1-dependent dehydrodimers or other factors such as chemical modifications, cellular localization, or optical effects.

Bathing leaf tissues in a highly osmotic solution uncovered that the BG fluorescence was localized within the shrinking protoplast (Figure S2C,D). Hence, dehydrodimers mainly arise in the vacuoles or the cytoplasm. We further analyzed in more detail the bright blue fluorescence at the lesion edges by confocal laser scanning microscopy (CLSM) that revealed a major source of UV-excited fluorescence at contact sites between epidermis cells and dying mesophyll cells (Figure 3j–l, Movies 1 and 2). Burst chloroplasts in the mesophyll always co-localized with bright blue fluorescence.

2.4 | Phenylpropanoid dehydrodimers function in inducible cell wall cross-linking during the HCD

It was shown before that dehydrodimers are bound to the cell wall by esterification (Buanafina, 2009; Ralph et al., 2004). To test whether this also occurs in Arabidopsis, we saponified cell wall fractions and analyzed the extracted esters by ultra performance liquid

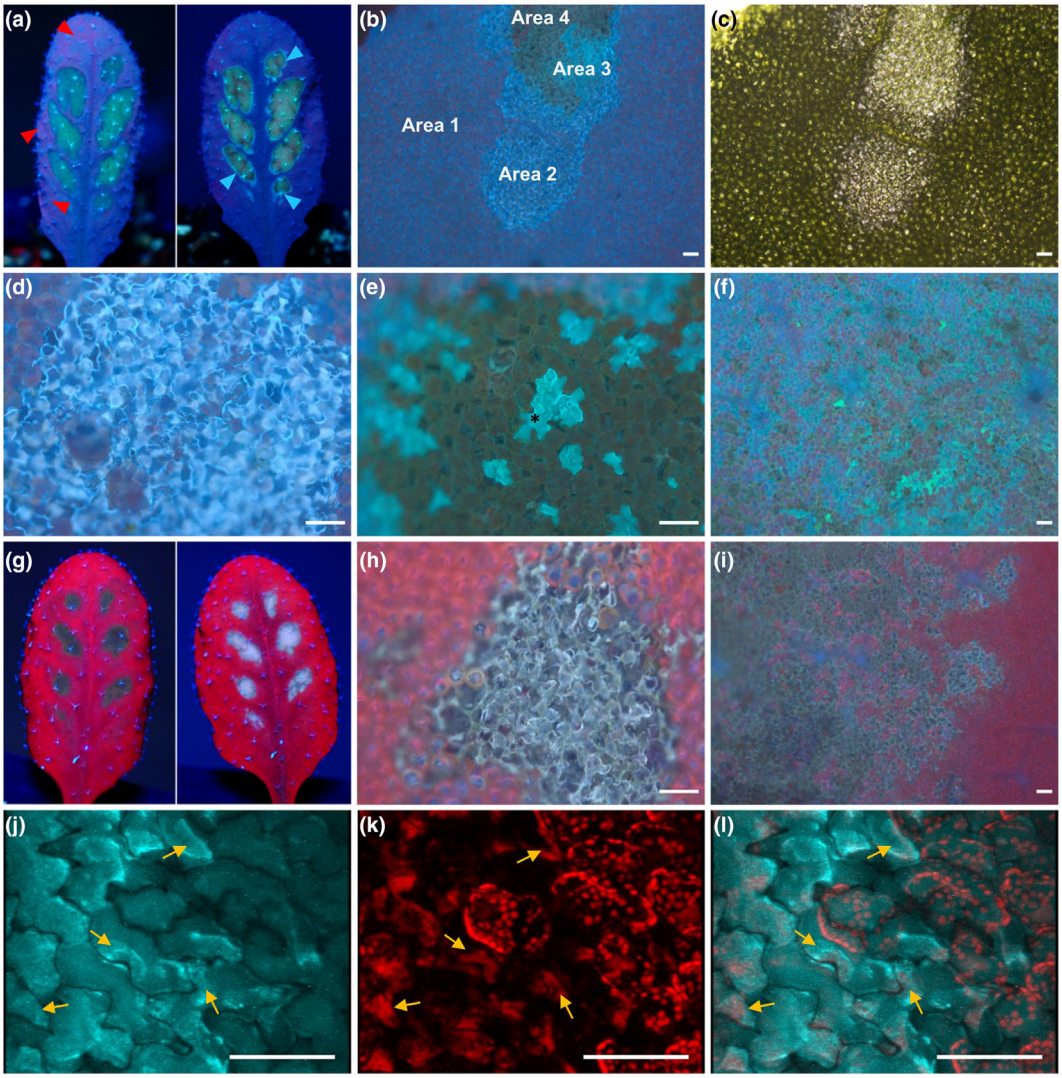

FIGURE 3 Hypersensitive cell death (HCD)-related blue-green (BG) and bright blue fluorescence is mainly localized in upper epidermal cells next to dying mesophyll cells. UV-induced fluorescence imaging by (a and g) a handheld UV lamp plus camera, (b–f, h, and i) fluorescence microscope, and (j–l) confocal laser scanning microscope (CLSM). HCD was triggered by fumigation with 30-ppm NO_2 for 20 min or infection with *Pseudomonas syringae* pv. *tomato* (*P.s.t. AvRpm1*). (a) Leaf of a wild-type (WT) plant at 4 h (left panel) and 24 h (right panel) after NO_2 exposure. Note the transiently enhanced red chlorophyll fluorescence at 4 h (red arrow heads) and the bright blue fluorescence (blue arrow heads) surrounding the lesions at 24 h after treatment. (b) Fluorescence emission under UV-A (365 nm) excitation. Weak blue fluorescence was visible in unaffected tissues (Area 1). Within the lesion, epidermal cells fluoresced bright blue (Area 2) or BG (Area 3). Dead tissue appeared brown (Area 4). (c) Transmission light revealed the chlorosis of mesophyll cells within the lesion. (d) HCD-related bright blue fluorescence was strongest in the peripheries of epidermal cells. (e) During HCD progression, fluorescence in epidermal cells turned BG and subsequently vanished. For instance, the cell highlighted by an asterisk was already partially transparent. Dead epidermis cells were transparent but mesophyll cells brown probably due to chlorophyll degradation products. (f) *P.s.t. AvrRpm1*-induced fluorescence in WT at 24 h after infection. BG and bright blue fluorescence was absent in *fah1* undergoing (g and h) NO_2-induced or (i) *P.s.t. AvrRpm1*-induced HCD. (j–l) Tissue at the lesion edges was examined by CLSM. (j) Localization of bright blue fluorescence (excitation at 364 nm/emission at ≥385 nm) and (k) red chlorophyll fluorescence (exc. at 633 nm/emi. at ≥650 nm) and (l) digital overlay of both (arbitrary colors). (j–l) Bright blue fluorescence often appeared at contact sites (arrows) of epidermis cells with mesophyll cells undergoing programmed cell death (PCD) as evidenced by broken chloroplasts. However, the bright blue fluorescence did not turn up in mesophyll cells or in epidermis cells next to live mesophyll cells with intact chloroplasts (refer also to Movies 1 and 2). Scale bars indicate 100 μm.

chromatography-tandem MS (UPLC–MS/MS). HCD induction by NO_2 or *P.s.t. AvrRpm1* caused the attachment of SM-SM, SM-Si, and Si-Si to the cell wall via ester bonds, whereas these dimers were not detected in leaf extracts from control plants (Figure 4a). Ferulate appeared to be a constitutive cell wall ester not showing upregulated levels upon HCD induction (Figure 4a). SM-SM esterified completely

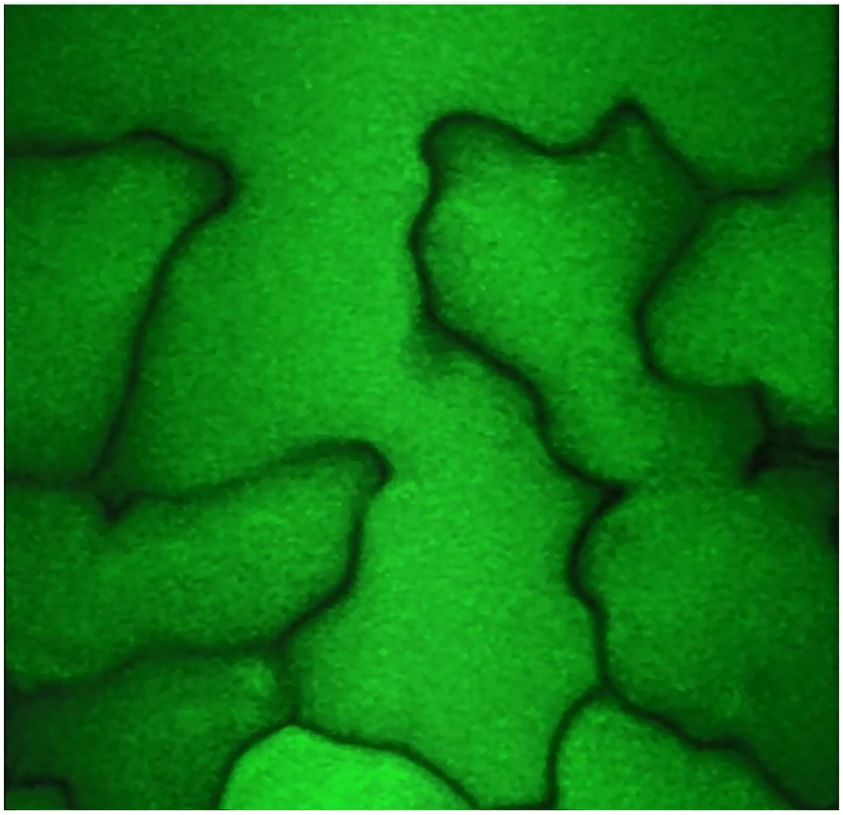

MOVIE 1 Localization of fluorescence in untreated leaf tissues by confocal laser scanning microscopy. Epidermal peels of air fumigated leaves were analyzed. Blue fluorescence was detected upon UV excitation (excitation at 364 nm/emission at ≥385 nm). Red chlorophyll fluorescence was detected at emission wavelengths ≥650 nm after excitation at 633 nm. Stacks of optical sections were used to prepare 3D videos.
Video content can be viewed at https://onlinelibrary.wiley.com/doi/10.1002/pld3.531

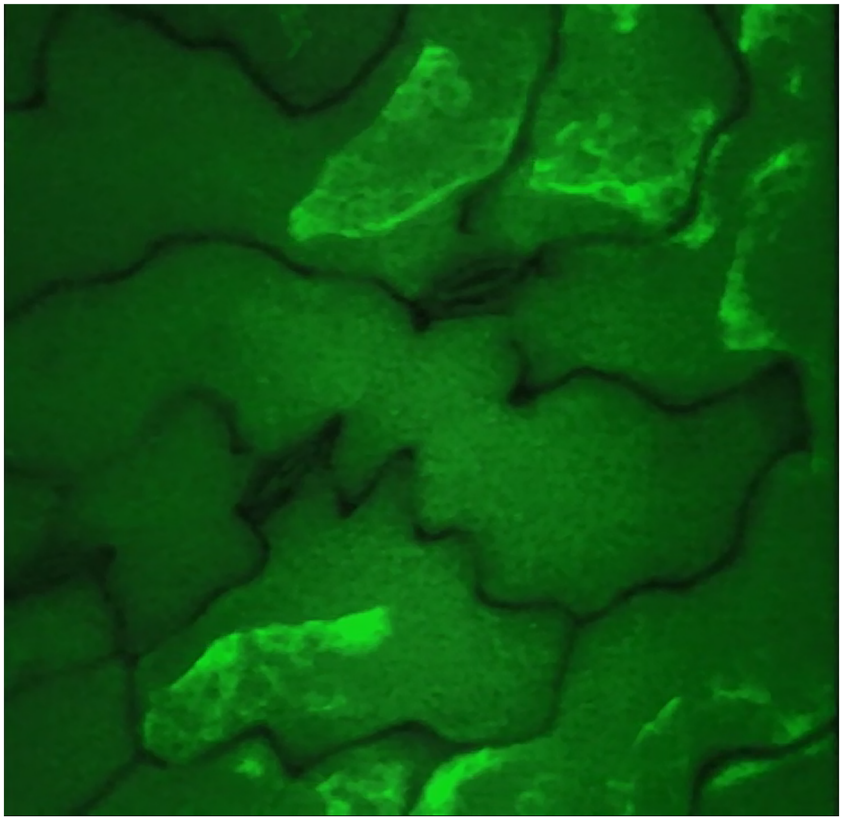

MOVIE 2 Localization of hypersensitive cell death (HCD)-related blue-green (BG) fluorescence by confocal laser scanning microscopy. Epidermal peels of NO_2-fumigated leaves were analyzed. Blue fluorescence was detected upon UV excitation (excitation at 364 nm/emission at ≥385 nm). Red chlorophyll fluorescence was detected at emission wavelengths ≥650 nm after excitation at 633 nm. Stacks of optical sections were used to prepare 3D videos. Note that burst chloroplasts in the mesophyll co-localize with bright fluorescence in collapsed epidermis cells. There is no bright fluorescence visible next to intact chloroplasts.
Video content can be viewed at https://onlinelibrary.wiley.com/doi/10.1002/pld3.531

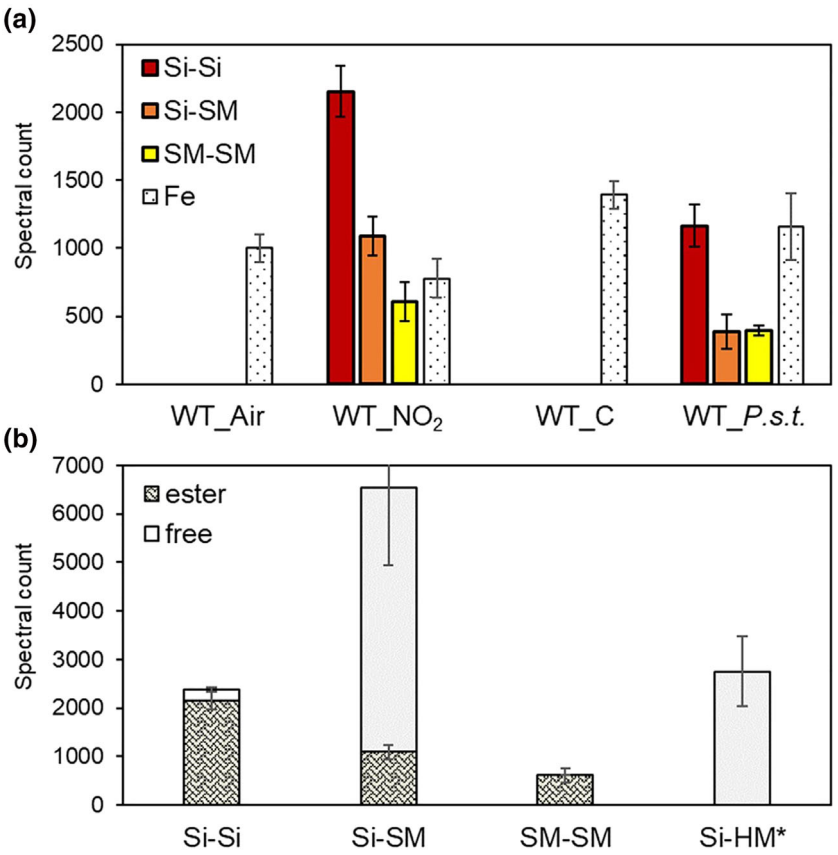

FIGURE 4 Dehydrodimers partially esterify to the cell wall during the hypersensitive cell death (HCD). (a) Ferulate (Fe), the dehydrodimers of sinapic acid (Si), sinapoylmalate (SM), and 5-hydroxyferuloylmalate (HM), namely, Si-Si, Si-SM, SM-SM, and Si-HM, were released from purified cell wall material by saponification before analysis by ultra performance liquid chromatography-tandem mass spectrometry (UPLC-MS/MS). Semi-quantification of dehydrodimer esters in wild-type (WT) plants 24 h after fumigation with 20-ppm NO_2 (vs. air as control) or infection with avirulent *Pseudomonas syringae* pv. *tomato* (*P.s.t.* vs. C, Control). (b) Some dehydrodimers only partially or not at all esterified to the cell wall within 24 h after NO_2 fumigation as revealed by comparing cell wall saponification extracts (ester) with soluble extracts (free). Error bars depict standard deviations ($n = 6$).

and Si-Si as well as Si-SM partially to cell wall polymers, whereas SM-Hf/Si-HM accumulated exclusively in its free form until 24 h after NO_2 treatment (Figure 4b).

3 | DISCUSSION

Dehydrodimers of sinapates and 5-hydroxyferulates are sources of the enigmatic BG fluorescence emerging during the HCD in Arabidopsis, which is supported by three observations: (i) The Si- and Hf-deficient mutant *fah1* does not exhibit BG fluorescence. (ii) Dehydrodimers are the only metabolites that accumulate during the HCD in a FAH1-dependent manner. (iii) Laccase-mediated oligomerization of Si in vitro causes a shift from blue to BG fluorescence as it also occurs in dying epidermis cells.

Previous research focussed mainly on dehydrodimers of ferulates, whereas much less is known about dimers of sinapates (Buanafina, 2009; Bunzel et al., 2003; Santiago & Malvar, 2010). Dehydrodiferulates facilitate cell wall cross-linking during growth and development (Buanafina, 2009; Ralph et al., 2004). Available evidence additionally argues for a role of these molecules in plant defense responses. For example, in different maize cultivars, the levels of dehydrodiferulates exhibited a positive correlation with resistance against the fungal pathogen *Fusarium graminearum* (Bily et al., 2003). Ikegawa et al. (1996) observed an increased esterification of hemicellulose by dehydrodiferulates during the HR of oat (*Avena sativa*) toward *Puccinia coronata* f.sp. *avenae*. And transgenic *Brachypodium distachyon* expressing a fungal ferulic acid esterase had reduced levels of ferulate and diferulate esters corresponding with an enhanced susceptibility to *Botrytis cinerea* (Reem et al., 2016).

Our current research provides new insights in the inducible formation of phenylpropanoid dehydrodimers during Arabidopsis defense responses. HCD induction did not cause the dimerization of ferulates in Arabidopsis. Instead of that, UV protectant sinapates and 5-hydroxyferulates were repurposed to form the dehydrodimers Si-Si, Si-SM, SM-SM, Si-Hf, Si-HM/SM-Hf, and SM-HM. Except for Si-Si,-none of these phenylpropanoid dehydrodimers has been identified before. Analogous to reported functions of diferulates in monocots, these molecules could promote rapid cell wall cross-linking in the upper epidermis although this hypothesis remains to be investigated. Future research will also reveal whether highly abundant phenylpropanoids in other plant species such as syringaldehyde and chlorogenic acid in lettuce (Bennett et al., 1996) dimerize during the HCD.

In grasses, ferulate monomers esterify the cell wall at arabinose O-5 positions of arabinoxylan side chains. Subsequent oxidative coupling of two wall-bound ferulate monomers has been proposed to cause the cross-linking of xylan chains (Buanafina, 2009; Ralph et al., 2004). However, according to our recent research in Arabidopsis, dehydrodimers arise from free monomers of sinapates and 5-hydroxyferulates and are subsequently attached to polysaccharides, which then could cause cross-linking. The exact localization of dehydrodiferulate formation is still debated. Dimers might form

intracellularly, extracellularly, and/or *in muro* (Buanafina, 2009; Lindsay & Fry, 2008). We found a strong intracellular source of BG fluorescence arguing for dimerization of sinapates and 5-hydroxyferulates within the upper epidermis cells. In addition to the prominent BG fluorescence, an FAH1-dependent bright blue fluorescence appeared at the lesion edges. CLSM uncovered that burst chloroplasts in dying mesophyll cells always co-localized with spots of bright blue-fluorescence in nearby epidermis cells. The disrupted photosynthesis in dying chloroplasts would lead to photooxidative stress involving the accumulation of reactive oxygen species (Asada, 2006). We hypothesize that this could contribute to the formation of dehydrodimers at contact sites between dying mesophyll- and epidermis cells.

Individual dehydrodimers exhibited markedly different wall-binding kinetics. Si-Si and SM-SM mostly esterified to the cell wall, whereas the pools of Si-SM remained largely and Si-HM/SM-Hf completely unbound until 24 h after onset of the HCD. These findings point to specific yet unknown functions of free versus wall-bound dehydrodimers. We did not detect diferulate in Arabidopis. Wall-bound ferulate monomers were not regulated during the HCD indicating that they might contribute to cell wall cross-linking during growth and development rather than defense responses.

In conclusion, HCD induction leads to the rapid formation of BG fluorescent dehydrodimers from large pre-existing pools of UV protectant Si and Hf derivatives within dying epidermis cells. The dimerization is spatially associated with burst chloroplasts in the mesophyll. At least a proportion of the dimers Si-Si, Si-SM, and SM-SM move into the apoplast where they bind to cell wall polymers by esterification thereby turning non-fluorescent. Dehydrodimer formation is not essential for the execution of HCD but is probably related to cell wall reinforcement. Future research will reveal functions of free and cell wall-bound phenylpropanoid dehydrodimers during the HCD.

4 | MATERIALS AND METHODS

4.1 | Plant material and HCD induction

A. thaliana ecotype Columbia-0 (Col-0), transgenic *pDex::AvrRpm1-HA* (Mackey et al., 2002), *fah1* (Chapple et al., 1992), and *pal1 pal2* (Rohde et al., 2004) plants were grown for 4–5 weeks on soil under long-day conditions as described previously (Kasten et al., 2016). Plants were exposed to 30-ppm NO_2 for 1 h or 20 min. Please refer to Mayer et al. (2018) and Kasten et al. (2017) for more details on the fumigation system used. *pDex::AvrRpm1-HA* plants were sprayed until run-off with 30-μM dexamethasone (Sigma) dissolved in .1% methanol/.01% Tween 20. As a negative control, plants were treated with methanol/Tween. Furthermore, we triggered HR-PCD by infection with *P.s.t.* carrying the avirulence gene *AvrRpm1* as described earlier (Gaupels et al., 2011).

4.2 | Fluorescence imaging

The imaging of BG autofluorescence in whole plants and leaves was done as reported before (Mayer et al., 2018). For microscopic examinations, the upper side of the leaf was opened by shallow vertical cuts. Subsequently, strips of the adaxial epidermis attached to mesophyll cells were peeled off using forceps and immediately mounted on a microscope slide in water. Occasionally, water was replaced by 50% glycerol solution to induce protoplast shrinking. An Olympus BX61 fluorescence microscope equipped with a XC50 camera served to define the tissue localization of the red and BG fluorescence. Fluorescence was excited with the 365-nm band of the UV laser and detected after passing a UV longpass filter. Additionally, we investigated epidermal peels with a Zeiss LSM 510 Meta CLSM. Here, the microscope setup included a 364-nm excitation laser combined with a 385-nm longpass filter for the detection of BG fluorescence or a 633-nm excitation laser combined with a 650-nm longpass filter for the detection of red fluorescence. The Zeiss ZEN lite and arivis Vision4D software facilitated the preparation of stacks, other figures, and 3D videos.

4.3 | 12-Tesla FT-ICR-MS and MS/MS fragmentation analysis

Metabolite extraction and FT-ICR-MS measurements followed published protocols (Kanawati et al., 2017; Mayer et al., 2018). However, for statistical analysis, we used in the R software package the beta-binomial test instead of the Wilcoxon rank sum test. MS/MS fragmentation experiments were performed by the use of Argon as an inert collision gas in a collision cell (hexapole) having a relatively high pressure of 3×10^{-6} mbar, when compared with the base pressure inside the ICR cell (1.5×10^{-10} mbar). No nozzle-skimmer dissociation or declustering potential inside the electrospray source was applied. Only slight standard linear ion acceleration of 3 eV was applied (prior to adding over it the MS/MS collision energy for MS/MS). This is necessary to forward the externally generated ions along the different linear ion beam guides toward the ICR cell.

4.4 | MDN analysis

MDN analysis was performed based on previous work (Moritz et al., 2016, 2019; Tziotis et al., 2011) by utilizing a home-made algorithm. First, it was determined whether accurate masses were linked by mass difference units corresponding to binding of dehydrogenated Si ($C_{11}H_{10}O_5$, 222.052823), SM ($C_{15}H_{14}O_9$, 338 .063782), 5-hydroxyferulic acid ($C_{10}H_8O_5$, 208.037173), 5-hydro xyferuloylmalate ($C_{14}H_{12}O_9$, 324.048132), ferulic acid ($C_{10}H_8O_4$, 192.042259), and feruloylmalate ($C_{14}H_{12}O_8$, 308.053217) (File S1). Subsequently, MDNs were visualized by the Gephi software (version 0.9.2, https://gephi.org/).

4.5 | Laccase assay

Fifty-millimolar sodium acetate (pH 5.0) containing or not (control) laccase from *Trametes versicolor* (Sigma) at a total activity of .004 U was prepared. Subsequently, 50 µl of 50-mM sinapate in DMSO was added to 1-ml laccase solution, and the reaction was placed in a shaker incubator at 50°C for 10 min. After centrifugation for 10 min at 16.000 ***g*** and RT, 100-µl sample was transferred to a 96-well plate. In a plate reader photometer, the fluorescence was recorded between 400 and 600 nm upon excitation at a wavelength of 320 nm.

4.6 | UPLC-MS/MS

The phenolic cell wall esters were extracted as reported earlier (Schnitzler et al., 1996) with minor modifications. We weighed 100–150 mg of frozen leaf material in 1.5-ml polypropylene tube containing 11–12 glass pearls. Leaf material was homogenized using the Silamat S6 bead mill (Ivoclar Vivadent) (Mayer et al., 2018). The weight of the tubes containing the glass beads was determined before and after adding leaf material and after air-drying of the washed insoluble leaf material to assess the amount of crude cell wall in each sample. Crude cell wall was prepared as follows: (i) Extraction with 1-ml methanol at room temperature in the dark for 1 h, subsequent centrifugation at 16,000 ***g*** for 10 min at 4°C, and two washings of cell debris with 1-ml MeOH. (ii) Sequential washings of cell debris by incubation for 20 min with each 1 ml of 1-M NaCl, .5% (w/v) SDS, and chloroform/methanol (1:1, v/v) followed by centrifugation (16,000 ***g*** for 10 min at 4°C). (iii) Final washing with acetone and air-drying of the crude cell wall material. For saponification, cell wall material was incubated in .5-ml 1-M NaOH for 16 h at room temperature in the dark followed by centrifugation. Samples were prepared by mixing 200-µl aliquots of the supernatants with 200-µl 1.5-M formic acid (centrifugation as above). SM was highly abundant in soluble extracts but absent from cell wall extracts confirming that the washings successfully removed soluble phenylpropanoids (Figure S3).

The samples were analyzed by metabolomics using UPLC Ultra-High Resolution (UHR) tandem quadrupole/Time-of-Flight (QqToF) mass spectrometry (MS). The LC-MS system was composed of an Ultimate 3000RS (Thermo Fisher) coupled to a Bruker Impact II with Apollo II electrospray ionization source (Bruker Daltonic). For the separation of polar cell wall esters, we used the hydrophilic interaction liquid chromatography (HILIC) column ACQUITY BEH Amide (Waters, 100 × 2.1 mm i.d. with 1.7-µm particles) with a gradient of solvent A (formic acid/water 99.9:.1 [v/v]) and solvent B (acetonitrile/formic acid 99.9:.1 [v/v]) following the gradient program depicted in Table S1.

Mass calibration was performed with the calibration mixture of 50 ml of water, 50-ml 2-propanol, 1-ml NaOH, and 200 µl of formic acid. The sample material was analyzed using MS in negative electrospray ionization mode using the following parameters: nebulizer pressure, 2.0 bar; dry gas flow, 8.0 L/min; dry gas temperature, 200°C; capillary voltage, 3500 V; endplate offset, 500 V; mass range, 20–2000 *m/z*. Smart exclusion feature together with the auto MS/MS acquisition mode was used for the precursor selection. The rolling average is used as a criterion to determine if the precursor is taken for MS/MS. When the difference between the rolling average of the set number of spectra and actual spectra is over the absolute threshold of 500 counts, the precursor is taken for MS/MS. A collision energy from 5 to 20 eV was used to obtain fragmentation of the ions.

The data were processed by the Metaboscape 4.0 software (Bruker). Processed data were given as "bucket" list containing the exact compound mass, isotope composition, and chemical clusters in each bucket. The detailed parameters for the software are given in the Table S1. The specific masses were found from the bucket list and assigned with the sum formula using the build it feature. The condition for the formula assignment was 5.0-mDa tolerance for the precursor mass. The missing values were replaced with the average area value from all samples for the corresponding mass feature (Denkert et al., 2006).

AUTHOR CONTRIBUTIONS

F.G., J.D., J.-P.S., and P.S.-K. designed the experiments. B.K., F.G., M.B., F.H., and I.Z. performed the experiments. B.K., M.B., F.H., and F.M. analyzed the data. F.G., P.S.-K., and D.M. wrote and critically revised the manuscript.

ACKNOWLEDGMENTS

We thank Elisabeth Georgii for support with the statistical analysis. Open Access funding enabled and organized by Projekt DEAL.

CONFLICT OF INTEREST STATEMENT

No conflict of interest declared.

DATA AVAILABILITY STATEMENT

The data that support the findings of this study are available in the supplementary material of this article.

ORCID

Marko Bertic https://orcid.org/0000-0001-9016-0902
Felix Habermann https://orcid.org/0000-0003-2916-3463
Ina Zimmer https://orcid.org/0000-0002-6441-8495
David Mackey https://orcid.org/0000-0002-0891-3061
Jörg-Peter Schnitzler https://orcid.org/0000-0002-9825-867X
Jörg Durner https://orcid.org/0000-0003-4436-4415
Frank Gaupels https://orcid.org/0000-0002-6079-6800

REFERENCES

Asada, K. (2006). Production and scavenging of reactive oxygen species in chloroplasts and their functions. *Plant Physiology*, *141*, 391–396. https://doi.org/10.1104/pp.106.082040

Bennett, M., Gallagher, M., Fagg, J., Bestwick, C., Paul, T., Beale, M., & Mansfield, J. (1996). The hypersensitive reaction, membrane damage and accumulation of autofluorescent phenolics in lettuce cell challenged by *Bremia lactucae*. *The Plant Journal*, *9*, 851–865. https://doi.org/10.1046/j.1365-313X.1996.9060851.x

Bily, A. C., Reid, L. M., Taylor, J. H., Johnston, D., Malouin, C., Burt, A. J., Bakan, B., Regnault-Roger, C., Pauls, K. P., Arnason, J. T., & Philogène, B. J. R. (2003). Dehydrodimers of ferulic acid in maize grain pericarp and aleurone: Resistance factors to *Fusarium graminearum*. *Phytopathology*, *93*, 712–719. https://doi.org/10.1094/PHYTO.2003.93.6.712

Buanafina, M. M. (2009). Feruloylation in grasses: Current and future perspectives. *Molecular Plant*, *2*, 861–872. https://doi.org/10.1093/mp/ssp067

Bunzel, M. (2010). Chemistry and occurrence of hydroxycinnamate oligomers. *Phytochemistry Reviews*, *9*, 47–64. https://doi.org/10.1007/s11101-009-9139-3

Bunzel, M., Ralph, J., Kim, H., Lu, F., Ralph, S. A., Marita, J. M., Hatfield, R. D., & Steinhart, H. (2003). Sinapate dehydrodimers and sinapate-ferulate heterodimers in cereal dietary fiber. *Journal of Agricultural and Food Chemistry*, *51*, 1427–1434. https://doi.org/10.1021/jf020910v

Chapple, C., Vogt, T., Ellis, B., & Somerville, C. (1992). An Arabidopsis mutant defective in the general phenylpropanoid pathway. *Plant Cell*, *4*, 1413–1424.

Coll, N. S., Epple, P., & Dangl, J. L. (2011). Programmed cell death in the plant immune system. *Cell Death and Differentiation*, *18*, 1247–1256. https://doi.org/10.1038/cdd.2011.37

Delledonne, M., Zeier, J., Marocco, A., & Lamb, C. (2001). Signal interactions between nitric oxide and reactive oxygen intermediates in the plant hypersensitive disease resistance response. *Proceedings of the National Academy of Sciences of the United States of America*, *98*, 13454–13459. https://doi.org/10.1073/pnas.231178298

Denkert, C., Budczies, J., Kind, T., Weichert, W., Tablack, P., Sehouli, J., Niesporek, S., Könsgen, D., Dietel, M., & Fiehn, O. (2006). Mass spectrometry–based metabolic profiling reveals different metabolite patterns in invasive ovarian carcinomas and ovarian borderline tumors. *Cancer Research*, *66*, 10795–10804. https://doi.org/10.1158/0008-5472.CAN-06-0755

Frank, U., Kublik, S., Mayer, D., Engel, M., Schloter, M., Durner, J., & Gaupels, F. (2019). A T-DNA mutant screen that combines high-throughput phenotyping with the efficient identification of mutated genes by targeted genome sequencing. *BMC Plant Biology*, *19*, 539. https://doi.org/10.1186/s12870-019-2162-7

Fraser, C. M., & Chapple, C. (2011). The phenylpropanoid pathway in Arabidopsis. *Arab B*, *9*, e0152. https://doi.org/10.1199/tab.0152

Frolov, A., Henning, A., Böttcher, C., Tissier, A., & Strack, D. (2013). An UPLC-MS/MS method for the simultaneous identification and quantitation of cell wall phenolics in *Brassica napus* seeds. *Journal of Agricultural and Food Chemistry*, *61*, 1219–1227. https://doi.org/10.1021/jf3042648

Gaupels, F., Kuruthukulangarakoola, G. T., & Durner, J. (2011). Upstream and downstream signals of nitric oxide in pathogen defence. *Current Opinion in Plant Biology*, *14*, 707–714. https://doi.org/10.1016/j.pbi.2011.07.005

Ikegawa, T., Mayama, S., Nakayashiki, H., & Kato, H. (1996). Accumulation of diferulic acid during the hypersensitive response of oat leaves to *Puccinia coronata* f.sp. avenae and its role in the resistance of oat tissues against cell wall degrading enzymes. *Physiological and Molecular Plant Pathology*, *48*, 254–256. https://doi.org/10.1006/pmpp.1996.0021

Kanawati, B., Bader, T. M., Wanczek, K.-P., Li, Y., & Schmitt-Kopplin, P. (2017). Fourier transform (FT)-artifacts and power-function resolution filter in Fourier transform mass spectrometry. *Rapid Communications in Mass Spectrometry*, *31*, 1607–1615. https://doi.org/10.1002/rcm.7940

Kasten, D., Durner, J., & Gaupels, F. (2017). Gas alert: The NO2 pitfall during NO fumigation of plants. *Frontiers in Plant Science*, *8*, 8–11. https://doi.org/10.3389/fpls.2017.00085

Kasten, D., Mithöfer, A., Georgii, E., Lang, H., Durner, J., & Gaupels, F. (2016). Nitrite is the driver, phytohormones are modulators while NO and H_2O_2 act as promoters of NO_2-induced cell death. *Journal of Experimental Botany*, *67*, 6337–6349. https://doi.org/10.1093/jxb/erw401

Katagiri, F., Thilmony, R., & He, S. Y. (2002). The *Arabidopsis thaliana-Pseudomonas syringae* interaction. *Arab B*, *1*, e0039. https://doi.org/10.1199/tab.0039

Lindsay, S. E., & Fry, S. C. (2008). Control of diferulate formation in dicotyledonous and gramineous cell-suspension cultures. *Planta*, *227*, 439–452.

Mackey, D., Holt, B. F., Wiig, A., & Dangl, J. L. (2002). RIN4 interacts with *Pseudomonas syringae* type III effector molecules and is required for RPM1-mediated resistance in Arabidopsis. *Cell*, *108*, 743–754. https://doi.org/10.1016/S0092-8674(02)00661-X

Mayer, D., Mithöfer, A., Glawischnig, E., Georgii, E., Ghirardo, A., Kanawati, B., Schmitt-Kopplin, P., Schnitzler, J. P., Durner, J., & Gaupels, F. (2018). Short-term exposure to nitrogen dioxide provides basal pathogen resistance. *Plant Physiology*, *178*, 468–487. https://doi.org/10.1104/pp.18.00704

Milkowski, C., & Strack, D. (2010). Sinapate esters in brassicaceous plants: Biochemistry, molecular biology, evolution and metabolic engineering. *Planta*, *232*, 19–35. https://doi.org/10.1007/s00425-010-1168-z

Moritz, F., Hemmler, D., Kanawati, B., Schnitzler, J.-P., & Schmitt-Kopplin, P. (2019). Chapter 12 - Mass differences in metabolome analyses of untargeted direct infusion ultra-high resolution MS data. In B. Kanawati & P. Schmitt-Kopplin (Eds.), *Fundam. Appl. Fourier Transform Mass Spectrom* (pp. 357–405). Elsevier.

Moritz, F., Kaling, M., Schnitzler, J.-P., & Schmitt-Kopplin, P. (2016). Characterization of poplar metabotypes via mass difference enrichment analysis. *Plant, Cell & Environment*, *40*, 1057–1073. https://doi.org/10.1111/pce.12878

Nicholson, R. L., & Hammerschmidt, R. (1992). Phenolic compounds and their role in disease resistance. *Annual Review of Phytopathology*, *30*, 369–389. https://doi.org/10.1146/annurev.py.30.090192.002101

Ralph, J., Bunzel, M., Marita, J. M., Hatfield, R. D., Lu, F., Kim, H., Schatz, P. F., Grabber, J. H., & Steinhart, H. (2004). Peroxidase-dependent cross-linking reactions of p-hydroxycinnamates in plant cell walls. *Phytochemistry Reviews*, *3*, 79–96. https://doi.org/10.1023/B:PHYT.0000047811.13837.fb

Reem, N. T., Pogorelko, G., Lionetti, V., Chambers, L., Held, M. A., Bellincampi, D., & Zabotina, O. A. (2016). Decreased polysaccharide feruloylation compromises plant cell wall integrity and increases susceptibility to necrotrophic fungal pathogens. *Frontiers in Plant Science*, *7*, 1–15. https://doi.org/10.3389/fpls.2016.00630

Rohde, A., Morreel, K., Ralph, J., Goeminne, G., Hostyn, V., de Rycke, R., Kushnir, S., Van Doorsselaere, J., Joseleau, J. P., Vuylsteke, M., et al. (2004). Molecular phenotyping of the pal1 and pal2 mutants of *Arabidopsis thaliana* reveals far-reaching consequences on phenylpropanoid, amino acid, and carbohydrate metabolism. *Plant Cell*, *16*, 2749–2771. https://doi.org/10.1105/tpc.104.023705

Santiago, R., & Malvar, R. A. (2010). Role of dehydrodiferulates in maize resistance to pests and diseases. *International Journal of Molecular Sciences*, *11*, 691–703. https://doi.org/10.3390/ijms11020691

Schnitzler, J. P., Jungblut, T. P., Heller, W., Köfferlein, M., Hutzler, P., Heinzmann, U., Schmelzer, E., Ernst, D., Langebartels, C., & Sandermann, H. (1996). Tissue localization of u.v.-B-screening pigments and of chalcone synthase mRNA in needles of Scots pine seedlings. *The New Phytologist*, *132*, 247–258. https://doi.org/10.1111/j.1469-8137.1996.tb01844.x

Tufegdžić, S., Bogdanović, J., Maksimović, V., & Vučinić, Ž. (2005). Characterization of enzymatically synthesized diferulate. *Annals of the new York Academy of Sciences*, *1048*, 466–470. https://doi.org/10.1196/annals.1342.068

Tziotis, D., Hertkorn, N., & Schmitt-Kopplin, P. (2011). Kendrick-analogous network visualisation of ion cyclotron resonance Fourier transform mass spectra: Improved options for the assignment of elemental compositions and the classification of organic molecular complexity. *European Journal of Mass Spectrometry*, *17*, 415–421. https://doi.org/10.1255/ejms.1135

Yin, N. W., Wang, S. X., Jia, L. D., Zhu, M. C., Yang, J., Zhou, B. J., Yin, J. M., Lu, K., Wang, R., Li, J. N., & Qu, C. M. (2019). Identification and characterization of major constituents in different-colored rapeseed petals by UPLC-HESI-MS/MS. *Journal of Agricultural and Food Chemistry*, *67*, 11053–11065. https://doi.org/10.1021/acs.jafc.9b05046

SUPPORTING INFORMATION

Additional supporting information can be found online in the Supporting Information section at the end of this article.

How to cite this article: Kanawati, B., Bertic, M., Moritz, F., Habermann, F., Zimmer, I., Mackey, D., Schmitt-Kopplin, P., Schnitzler, J.-P., Durner, J., & Gaupels, F. (2023). Blue-green fluorescence during hypersensitive cell death arises from phenylpropanoid deydrodimers. *Plant Direct*, *7*(9), e531. https://doi.org/10.1002/pld3.531